Research Article | Vol. 11, No. 10 / 1 October 2020 / Biomedical Optics Express 5967
Biomedical Optics EXPRESS

Optical monitoring of cerebral perfusion and metabolism in adults during cardiac surgery with cardiopulmonary bypass

AJAY RAJARAM,[1,2,*] DANIEL MILEJ,[1] MARIANNE SUWALSKI,[1,2] LAWRENCE C. M. YIP,[1,2] LINRUI R. GUO,[4] MICHAEL W. A. CHU,[4] JASON CHUI,[3] MAMADOU DIOP,[1,2] JOHN M. MURKIN,[3] AND KEITH ST. LAWRENCE[1,2]

[1]*Imaging Program, Lawson Health Research Institute, 268 Grosvenor St., London, ON, N6A 4V2, Canada*
[2]*Department of Medical Biophysics, Western University, 1151 Richmond St., London, ON, N6A 3K7, Canada*
[3]*Department of Anesthesiology and Perioperative Medicine, London Health Science Centre, 339 Windermere Rd, London, ON, N6A 5A5, Canada*
[4]*Division of Cardiac Surgery, London Health Science Centre, 339 Windermere Rd, London, ON, N6A 5A5, Canada*
[*]*arajara2@uwo.ca*

Abstract: During cardiac surgery with cardiopulmonary bypass (CPB), adequate maintenance of cerebral blood flow (CBF) is vital in preventing postoperative neurological injury – i.e. stroke, delirium, cognitive impairment. Reductions in CBF large enough to impact cerebral energy metabolism can lead to tissue damage and subsequent brain injury. Current methods for neuromonitoring during surgery are limited. This study presents the clinical translation of a hybrid optical neuromonitor for continuous intraoperative monitoring of cerebral perfusion and metabolism in ten patients undergoing non-emergent cardiac surgery with non-pulsatile CPB. The optical system combines broadband near-infrared spectroscopy (B-NIRS) to measure changes in the oxidation state of cytochrome c oxidase (oxCCO) – a direct marker of cellular energy metabolism – and diffuse correlation spectroscopy (DCS) to provide an index of cerebral blood flow (CBFi). As the heart was arrested and the CPB-pump started, increases in CBFi ($88.5 \pm 125.7\%$) and significant decreases in oxCCO (-0.5 ± 0.2 μM) were observed; no changes were noted during transitions off CPB. Fifteen hypoperfusion events, defined as large and sustained reductions in CPB-pump flow rate, were identified across all patients and resulted in significant decreases in perfusion and metabolism when mean arterial pressure dropped to 30 mmHg or below. The maximum reduction in cerebral blood flow preceded the corresponding metabolic reduction by 18.2 ± 15.0 s. Optical neuromonitoring provides a safe and non-invasive approach for assessing intraoperative perfusion and metabolism and has potential in guiding patient management to prevent adverse clinical outcomes.

1. Introduction

Cardiopulmonary bypass (CPB) has become a cornerstone of cardiac surgery since its introduction in the 1950s. By taking over the physiological functions of the heart and lungs, CPB provides surgeons with an operating field unobstructed by blood and free of cardiac motion; however, there are numerous postoperative neurological complications associated, including cognitive dysfunction [1–3], delirium, and stroke [4–6]. During CPB, procedural changes in pump flow rate and unplanned fluctuations in cardiac output can produce variations in cerebral blood flow (CBF) [7]. Given the high metabolic demands of the brain and its reliance on a continuous supply

#404101 https://doi.org/10.1364/BOE.404101
Journal © 2020 Received 29 Jul 2020; revised 3 Sep 2020; accepted 3 Sep 2020; published 29 Sep 2020

Biomedical Optics EXPRESS

of oxygen, changes in CBF that are large enough to impact cerebral metabolism could lead to tissue damage and subsequent brain injury.

There is currently no established method for intraoperative monitoring of CBF and cerebral metabolism during CPB. Traditionally, CBF was measured using Xenon-133, a discontinuous method that requires an invasive injection via the arterial circulation [8]. Transcranial Doppler (TCD) ultrasound has also been used to measure CBF in major cerebral arteries [9]; however, TCD embodies numerous drawbacks, including space limitations when utilizing a large transducer probe, inconsistent acoustic windows due to variations in thickness and porosity of the skull [10], and signal contamination from electrocautery used during surgery [11]. Optical techniques are becoming more prevalent for real-time monitoring due to their safety, low-cost, and ease of implementation [12]. Cerebral oximetry can continuously measure cerebral tissue saturation (S_tO_2) during surgery and provides valuable insight into cerebral hemodynamics, but has proven insufficient for monitoring oxygen utilization [13–15]. More advanced optical methods of neuromonitoring have demonstrated the ability to measure microcirculatory blood flow and cerebral metabolism continuously and noninvasively [16,17]. Broadband near-infrared spectroscopy (B-NIRS) provides a means of directly monitoring cerebral energy metabolism by measuring the oxidation state of cytochrome c oxidase (oxCCO). This enzyme is involved in the electron transport chain and is vital to energy production via oxidative phosphorylation [18]. In addition, diffuse correlation spectroscopy (DCS) provides continuous CBF monitoring by tracking the temporal correlation of light scatter from red blood cells in the cerebral microvasculature [19–22].

This manuscript reports the clinical translation of a hybrid B-NIRS/DCS optical neuromonitor to provide non-invasive and continuous monitoring of CBF and oxCCO throughout cardiac surgery with CPB. The goal was to assess the system's ability to identify fluctuations in perfusion and metabolism, while determining the efficacy of CPB in maintaining adequate oxygen supply and utilization. It was hypothesized that transitions on and off CPB would impact CBF, based on the CPB-pump flowrate (FR_{CPB}) chosen, but fluctuations in flow would be insufficient to impact cerebral metabolism. It was also expected that significant operational changes in FR_{CPB}, while patients were fully reliant on CPB, would directly influence cerebral hemodynamics, with large and sustained drops leading to metabolic change.

2. Methods

2.1. Patient population

This study was approved by the Western University Health Sciences Research Ethics Board, which adheres to the guidelines of the Tri-Council Policy Statement: Ethical Conduct for Research Involving Humans (REB #113650). After obtaining consent, patients admitted to University Hospital's Cardiac Surgical Unit in London, Ontario, were monitored during non-emergent cardiac surgery with the use of non-pulsatile CPB.

2.2. Clinical monitoring

Optical monitoring was conducted throughout surgery with CPB. Vital parameters were recorded with a clinical unit (Intellivue MX800, Philips Healthcare, MA, USA) and exported to the optical system. In accordance with clinical protocol, patients presenting with an increased risk of postoperative cognitive effects were monitored with EEG and a cerebral oximeter (SedLine, Masimo, CA, USA). The optical probes were placed on the right temporal region of the forehead following anesthetic induction, endotracheal intubation, and placement of arterial and venous lines, but prior to skin incision. The probes were secured using a 3D-printed probe holder (Fig. 1(a)) and medical tape. Two optical fibers delivered light from the DCS and B-NIRS sources onto the patient's scalp. Diffusely reflected light was collected from a common detection

Biomedical Optics EXPRESS

fiber bundle that corresponded to source-detector distances (SDD) of 2 and 3 cm for DCS and B-NIRS, respectively (Fig. 1(b)), to ensure adequate brain interrogation. Prior to monitoring, broadband light spectra were assessed to ensure negligible contamination from ambient light and the Masimo oximeter (< 5% signal contribution). Optical source power levels were maintained within ANSI limits for skin exposure.

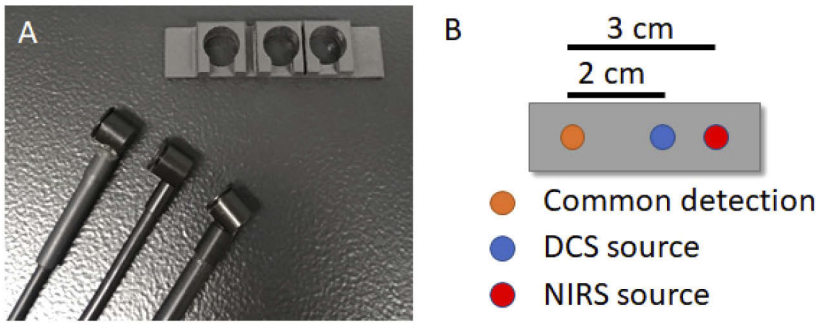

Fig. 1. A) Optical fiber probes and 3D-printed probe holder (5 × 2 × 1 cm) B) Schematic of the probe holder showing near-infrared spectroscopy (NIRS, 3-cm SDD) and diffuse correlation spectroscopy (DCS, 2-cm SDD) emission probes with a common detection probe.

B-NIRS and DCS measurements were acquired sequentially in a period of 3 s each. Within each period, the integration time was 250 ms. A transition delay of 0.5 s was incorporated between techniques to account for shutter transition times, achieving a cycle time of 7 s. Data were continuously acquired during the entire surgical procedure, spanning the transition on and off the CPB machine. Prior to and following CPB, DCS data were acquired for a minimum of 10 seconds at an increased sampling rate (20 Hz) to capture pulsatile waveforms.

2.3. Instrumentation

The development of a hybrid B-NIRS/DCS system has been previously reported and demonstrated continuous monitoring of cerebral blood flow, cerebral oxygen saturation, and metabolism in both animal models and infants in the neonatal intensive care unit [16,17].

The system was constructed by combining B-NIRS and DCS modalities using a multiplexing shuttering system. The B-NIRS source (Hl-2000-HP, Ocean Optics, FL, USA) was coupled into a custom optical fiber bundle (2.4 mm diameter active area, 30 µM core, 0.55 numerical aperture (NA), Loptek, Germany) to guide light to the subject's head. Light that interrogated the head was collected by a detection fiber bundle (2 mm diameter active area, 30 µm core, 0.55 NA, Loptek, Germany), and led to a custom-made spectrometer (548 to 1085 nm bandwidth; 1.65 nm resolution; P&P Optica, ON, Canada). Light from the DCS laser (DL785-100s, CrystaLaser, NV, USA) was similarly coupled into a fiber bundle (4 × 200 µm core diameter, 0.22 NA, Loptek, Germany) and directed towards the head. Diffusely reflected DCS light was collected with a bundle of four single-mode fibers (8 µm core diameter, 0.12 NA, Loptek, Germany) coupled to a four-channel single-photon counting module (SPCM-AQR-15-FC, Excelitas Technologies, QC, Canada). The output of the detectors was sent to a data acquisition board (PCIe-6612, National Instruments, TX, USA) and processed by in-house developed software (LabVIEW, National Instruments, TX, USA; MATLAB, MathWorks, MI, USA) [23,24]. Intensity autocorrelation curves at 50 delay times, ranging from 1 µs to 1 ms, were generated for each detector.

For use in the operating room, the fibers were shielded to prevent ambient light contamination from the bright surgical environment. The tips of the optical probes, in contact with the scalp, were bent 90 degrees to maintain a low profile and held in placed by a 3D-printed holder

Biomedical Optics EXPRESS

constructed from a lightweight, flexible material (5 × 2 × 1 cm; Flexible Resin, Form 2, Formlabs, MA, USA).

2.4. Data processing

2.4.1. B-NIRS quantification of baseline S_tO_2

Prior to clinical monitoring, the spectral profile of the optical system was characterized by acquiring a reference measurement. Once the probes were positioned on the scalp, a dark count measurement was acquired while the light sources of the optical system were off. A reflectance measurement R(λ) was determined by correcting for both reference and dark count measures as follows:

$$R(\lambda) = \log_{10}\left(\frac{spectrum_\lambda - dark_\lambda}{reference_\lambda - dark_\lambda}\right) \tag{1}$$

where spectrum_λ refers to the measured light intensity at wavelength λ. Reflectance data were analyzed by fitting the first and second derivatives of R(λ) to solutions of the diffusion approximation for a semi-infinite homogeneous medium [12,25,26]. As previously reported, the tissue water fraction, oxy- and deoxy-hemoglobin (HbO_2, Hb) concentrations, and scattering parameters were estimated using a three-step multi-parameter fitting with a constrained minimization algorithm based on the MATLAB function fminsearchbnd [12,16,17]. Baseline tissue oxygen saturation ($S_tO_2{}^b$) was calculated from the estimated hemoglobin concentrations:

$$S_tO_2{}^b = \frac{HbO_2{}^b}{Hb^b + HbO_2{}^b} \tag{2}$$

where the superscript b denotes baseline values.

2.4.2. Monitoring S_tO_2 and absolute change in oxidative state of cytochrome c oxidase

Following a minimum five-minute baseline measurement, a modified Beer-Lambert Law based on the UCLn algorithm (Eq. (3)) was used to calculate changes in Hb, HbO_2, and oxCCO concentrations [18].

$$\begin{bmatrix} \Delta HbO_2 \\ \Delta Hb \\ \Delta oxCCO \end{bmatrix} = \frac{1}{DP} \begin{bmatrix} \varepsilon_{HbO_2}(\lambda_1) & \varepsilon_{Hb}(\lambda_1) & \varepsilon_{oxCCO}(\lambda_1) \\ \vdots & \vdots & \vdots \\ \varepsilon_{HbO_2}(\lambda_n) & \varepsilon_{Hb}(\lambda_n) & \varepsilon_{oxCCO}(\lambda) \end{bmatrix}^{-1} \times \begin{bmatrix} \Delta A(\lambda_1) \\ \vdots \\ \Delta A(\lambda_n) \end{bmatrix} \tag{3}$$

where ΔHbO_2, ΔHb, and $\Delta oxCCO$ are the relative changes from baseline in oxy-hemoglobin, deoxy-hemoglobin, and the oxidation state of cytochrome c oxidase, respectively. DP is the differential pathlength and ΔA is the measured change in attenuation. DP was set to 6.26, based on previous literature representing measurements in the adult head [27], and corrected for the wavelength dependency of the pathlength [28]. Relative measures determined by the modified Beer-Lambert approach were utilized in conjunction with absolute baseline values from the derivative approach (section 2.4.1). This method provided absolute saturation values at faster computational speeds, allowing for real-time data interpretation. Tissue saturation was determined as follows [17]:

$$S_tO_2 = \frac{(HbO_2{}^b + \Delta HbO_2)}{(Hb^b + \Delta Hb) + (HbO_2{}^b + \Delta HbO_2)} \tag{4}$$

Biomedical Optics EXPRESS

2.4.3. CBF monitoring

Acquired DCS intensity data were normalized, autocorrelated, and converted to electric field autocorrelation data following the Siegert relation [29,30]. Each autocorrelation function was fit with the solution to the diffusion approximation for a semi-infinite homogenous medium for SDD = 2 cm, dynamic μ_a measurements obtained by B-NIRS, and a constant value for μ_s' of 8 cm^{-1} [22]. Fitting resulted in an estimate of the cerebral blood flow index (CBFi). CBFi data were normalized to baseline values to represent relative changes [31].

2.5. Statistical analysis

All data are presented as mean ± standard deviation and statistical significance is defined as $p < 0.05$. CPB transition periods were defined as the minimum time to increase the CPB-pump flow rate (FR_{CPB}) from zero to values sustained throughout the procedure, and vice-versa. To characterize this impact, data were averaged over 5-minute periods immediately surrounding CPB transitions and displayed in boxplots. An additional 5-minute period was analyzed 15 minutes into CPB and compared to baseline values. Outliers were defined as points greater than q3 + w × (q3 – q1) or less than q1 – w × (q3 – q1), where w represents the whisker length and q indicates quartile number. A two-tailed paired t-test was conducted to determine significance following the onset/end of CPB. Intraoperative hypoperfusion events were identified, defined as sudden and large decreases in FR_{CPB} lasting a minimum of 30 s. Changes in optical parameters during these events were binned into 10-mmHg MAP intervals and plotted. A multivariate ANOVA was used to determine statistical significance in optical parameters compared to baseline values. For each hypoperfusion event, the maximum reductions in CBFi and oxCCO were compared.

3. Results

Optical measurements were acquired in ten adult patients (nine male, one female, aged 34 to 76 years, mean age = 58.1 ± 13.8 years). Data from the first three patients had to be excluded due to excessive ambient light from the bright surgical environment. Additional shielding, in the form of an optical blackout cloth (Thorlabs, NJ, USA), was implemented following these subjects to minimize artifacts from external light sources (< 5% signal contribution). Data from the fourth and seventh patients were limited to hypoperfusion events due to excessive motion during CPB transitions. The fourth subject experienced the onset of a bleed in the chest cavity resulting in a severely deteriorating condition and ultimately death. Remaining data sets were analyzed for changes in CBFi, S_tO_2, and oxCCO. Table 1 displays patient demographics.

Figure 2 displays time courses from one patient during the transition on (Fig. 2(A)) and off (Fig. 2(B)) CPB; the FR_{CPB}, mean arterial pressure (MAP), and optical measurements – ΔCBFi, S_tO_2, and ΔoxCCO – are displayed. The FR_{CPB} was measured by the CPB machine and MAP with the clinical Philips monitor from a radial artery site.

As each patient was transitioned onto CPB, as indicated by the increase in the FR_{CPB}, and the heart was arrested using a potassium solution, blood flow changed from a pulsatile to non-pulsatile state. This is apparent in the standard deviation of CBFi; pulsatile flow produced a larger range of values (Fig. 2(A) < 8 min) compared to on-pump flow. The reverse effect was evident during the transition off CPB (Fig. 2(B) > 10 min) as the heart was restarted. Averaged values across all subjects during pre-, on-, and post-CPB periods are displayed in Table 2. Data represented as a change (Δ) were acquired for 5-minute intervals immediately surrounding the transition on CPB, 15 minutes into CPB, and immediately surrounding the transition off CPB. CPB transitions are represented in boxplots in Fig. 3. The average transition time on CPB was 202 ± 111 s, and off CPB was 230 ± 160 s. During the on-CPB transition, subjects showed a notable increase in CBFi and a statistically significant decrease in MAP and ΔoxCCO. No significant change persisted

Biomedical Optics EXPRESS

Table 1. Demographic and procedural variables[a]

Sex (n)	F = 1, M = 6
Age (year)	58.1 ± 13.8
Duration of surgery (min)	409.4 ± 191.4
Duration of CPB (min)	191.9 ± 177.3
Procedure (n)	
- CABG	3
- CABG + AVR	1
- Aortic arch repair	1
- Bentall	1
- Bentall + MVR	1
Patient death (n)	1

[a]CABG: Coronary artery bypass graft; AVR: Aortic valve replacement; MVR: Mitral valve replacement. Values are represented as mean ± standard deviation.

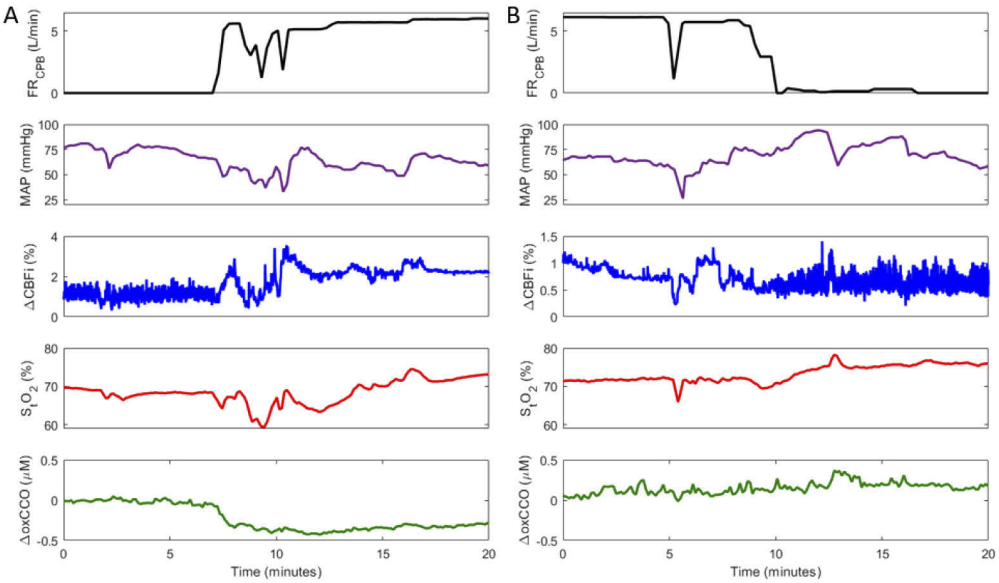

Fig. 2. Cerebral hemodynamics during transition A) on cardiopulmonary bypass (CPB) and B) off CPB. Figure shows a continuous measure of CPB-pump flowrate (FR_{CPB}), mean arterial pressure (MAP), change in the cerebral blood flow index (ΔCBFi), cerebral tissue saturation (S_tO_2), and changes in the oxidation state of cytochrome c oxidase (ΔoxCCO). ΔCBFi scales are adjusted across plots for data visualization.

Biomedical Optics EXPRESS

15 minutes into CPB. Following CPB, MAP increased, while CBFi and ΔoxCCO displayed no significant change. S_tO_2 remained stable throughout the procedure.

Table 2. Hemodynamic parameters throughout cardiopulmonary bypass (CPB)[a]

Parameter	Pre-CPB	On-CPB	Post-CPB
tHb (g/L)	112.6 ± 20.8	85.0 ± 13.0*	111.8 ± 42.8
pH	7.41 ± 0.06	7.33 ± 0.02*	7.38 ± 0.03
$PaCO_2$ (mmHg)	41.1 ± 3.9	35.3 ± 6.2	38.8 ± 1.5
Temperature (°C)	35.6 ± 0.4	33.6 ± 2.4	36.3 ± 0.5
Parameter	Transition on CPB	Mid-CPB	Transition off CPB
ΔMAP (mmHg)	-18.8 ± 11.3*	-6.0 ± 9.5	11.0 ± 21.8
ΔCBFi (%)	88.5 ± 125.7	51.9 ± 91.4	-3.3 ± 17.2
ΔS_tO_2 (%)	1.2 ± 5.2	-2.8 ± 5.7	1.4 ± 3.1
ΔoxCCO (μM)	-0.5 ± 0.2*	-0.3 ± 0.5	0.2 ± 0.3

[a]tHb: total Hemoglobin, $PaCO_2$: partial pressure of carbon dioxide. 'Transition on CPB' data were acquired as a change immediately surrounding CPB onset; 'Mid CPB' data were acquired 15 min following CPB onset and compared to pre-CPB data; 'Transition off CPB' data were acquired as a change immediately surrounding the end of CPB. Data were averaged over 5-minute intervals; * indicates statistical significance ($p < 0.05$).

CBFi data were also acquired at increased acquisition rate (20 Hz) prior to and following CPB. Figure 4 depicts fast blood flow monitoring in an aortic valve replacement (AVR) patient before

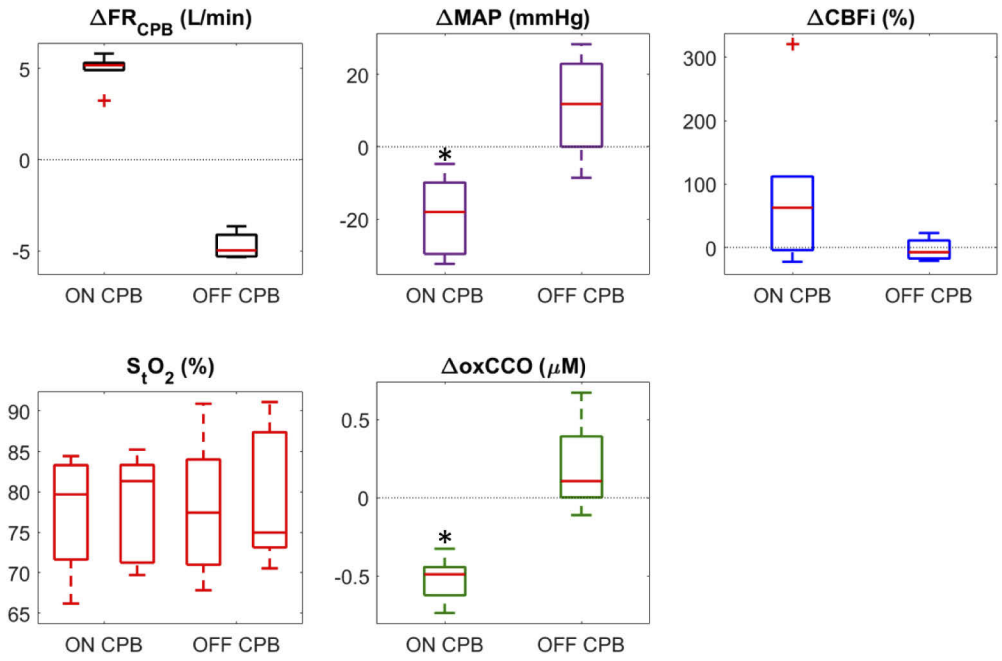

Fig. 3. Box plots showing average change across subjects during transitions onto the CPB pump (ON CPB) and off of the pump (OFF CPB). Absolute S_tO_2 values are shown for periods immediately before and after each transition. Data were averaged for 5-minute durations immediately surrounding the transition period; + indicates statistical outliers and * indicates a statistically significant difference across the transition. Average transition time on CPB was 202 ± 111 s, and off CPB was 230 ± 160 s.

Biomedical Optics EXPRESS

(Fig. 4(A)) and following (Fig. 4(B)) replacement of the defective valve. The increased sampling rate allowed for depiction of pulsatile waveforms within the CBFi measure. Following AVR, the range of CBFi values increased for each ejection and a change in the shape of the secondary peak – which represents a change in pressure due to vascular elastic recoil following AV closure – became apparent, indicating a potential improvement in flow and pressure dynamics within the heart [23,32].

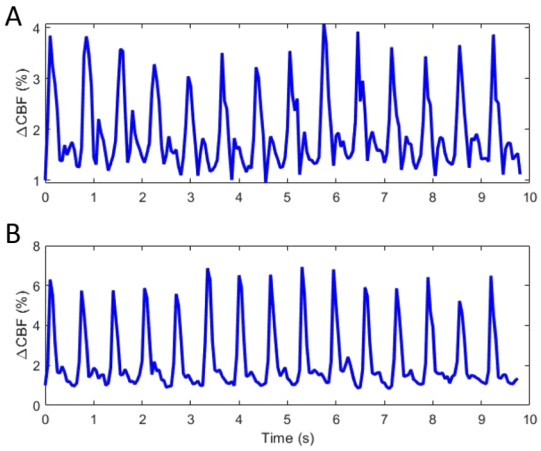

Fig. 4. Pulsatile waveforms observed in cerebral microcirculation measured at 20 Hz A) pre and B) post aortic valve replacement.

Across the seven patient data sets, 15 hypoperfusion events, defined as large decreases in FR_{CPB} (mean change 2.8 ± 1.4 L/min, $70.6 \pm 28.8\%$) and lasting a minimum of 30 seconds in duration (mean duration 93.9 ± 52.5 s), were observed. Figure 5 displays data acquired in subject four during a stable period (Fig. 5(A)) and when experiencing successive drops in FR_{CPB} (Fig. 5(B)). With a stable FR_{CPB}, no significant changes were detected in the optical parameters. In Fig. 5(b), the drop in ΔCBFi (~2.5-minute mark) coincides with the onset of a significant bleed during surgery. This event prompted immediate reductions in FR_{CPB} to allow for surgical correction. MAP and optical measures were found to mirror changes in FR_{CPB}, with S_tO_2 and ΔoxCCO displaying a delayed response compared to ΔCBFi.

Correlation plots of hypoperfusion events, showing changes in optical parameters as a function of MAP, are displayed in Fig. 6; statistical outliers are depicted by red crosses. Statistically significant changes in ΔCBFi occurred below MAP values of 30 mmHg, in S_tO_2 below 20 mmHg, and in ΔoxCCO between 30 to 20 mmHg and below 10 mmHg.

The maximum changes in oxCCO during each hypoperfusion event were plotted against the maximum change in CBFi in Fig. 7. A temporal delay of 18.2 ± 15.0 s was found between nadirs of ΔCBFi and ΔoxCCO. A delayed metabolic response in relation to flow has been previously reported [16,17,33,34]. Changes in CBFi greater than 70% resulted in large decreases in oxCCO.

Biomedical Optics EXPRESS

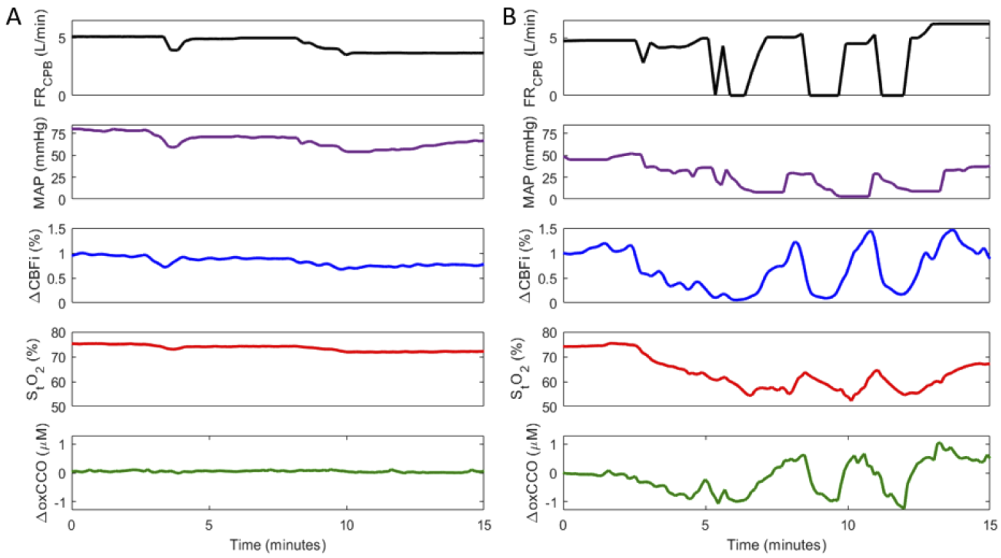

Fig. 5. Cerebral hemodynamics in subject 4 during A) a stable period and B) successive FR_{CPB}-driven hypoperfusion events. Each graph includes a continuous measure of CPB-pump flow rate (FRC_{CPB}), mean arterial pressure (MAP), change in cerebral blood flow (ΔCBFi), cerebral tissue saturation (S_tO_2), and changes in the oxidation state of cytochrome c oxidase (ΔoxCCO). Data were temporally averaged (7-s window) for visualization.

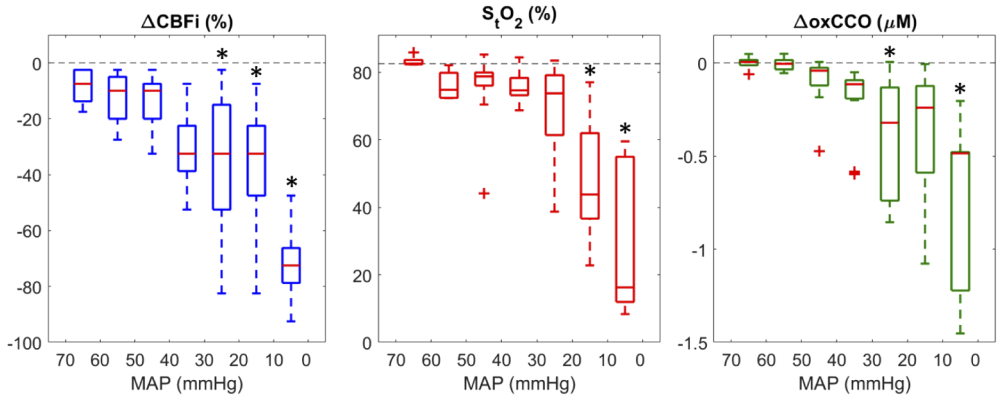

Fig. 6. Correlation boxplots of ΔCBF, S_tO_2, and ΔoxCCO as a function of MAP; + indicates statistical outliers and * indicates a statistically significant difference from baseline values.

Biomedical Optics EXPRESS

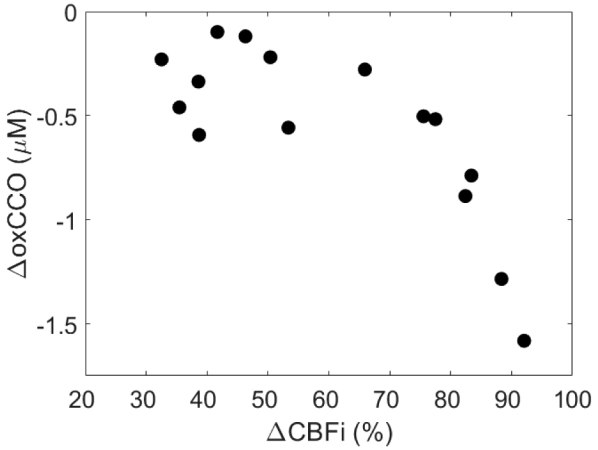

Fig. 7. Correlation plot showing the relationship between the maximum reductions in ΔCBFi and ΔoxCCO. On average, the ΔoxCCO nadir occurred 18.2 ± 15.0 s after the corresponding ΔCBFi nadir.

4. Discussion

For patients undergoing cardiac surgery with the use of CPB, current clinical standards are either completely absent of brain specific monitoring or reliant on commercial oximetry devices to provide regional cerebral oxygen saturation measurements. While oximetry has advanced to provide robust continuous measures, saturation alone has proven insufficient in describing metabolism and predicting neurological outcome [15,35]. The goal of this study was to test the feasibility of a newly developed optical brain monitor to provide intraoperative measurements of cerebral hemodynamics and metabolism during CPB.

In seven patients undergoing cardiac surgery with CPB, the hybrid optical device provided continuous monitoring of cerebral blood flow based on the DCS blood flow index (CBFi) and metabolism using B-NIRS to measure changes in the oxidation state of cytochrome c oxidase (ΔoxCCO). During transitions onto CPB (Fig. 2(A)), the FR_{CPB} was increased to provide adequate perfusion as the heart was arrested. The CPB pump was initially filled with a crystalloid solution in its reserve; when the pump was started, the first cycle was devoid of blood. As it continued, the crystalloid solution and blood mixed, resulting in a hemodilution effect that gradually diminished. From the perspective of the B-NIRS acquisition, there was a sudden change in the optical properties which may have contributed to the observed change in oxCCO. While Fig. 3 shows a statistically significant drop in ΔoxCCO, implying inadequate oxygen utilization across the on-CPB transition, the influence of hemodilution during this transition phase must be considered. It is also noteworthy that a significant increase in MAP was observed across this period and that no significant change in oxCCO persisted 15 minutes into CPB. Studies by Lassnigg et al. and Talpahewa et al. both reported similar changes in oxCCO following CPB-onset while noting contributions from hemodilution effects [36,37]. While hemodilution also results in a reduced number of moving light scatterers (e.g., red blood cells), it did not appear to have the same impact on DCS, since the CBFi measure relies on the temporal correlation of dynamic light scatter. Instead, CBFi was influenced to a greater extent by the FR_{CPB}. The clinically chosen FR_{CPB} was generally within a limited range from 2.0 to 2.5 L/min/m^2, using an estimated surface area for each patient [38–40]. Figure 3 displays a large range of ΔCBFi following CPB onset, with an average increase of 88.5 ± 125.7%. This shows that pump-flow rates were consistently overestimated, in relation to baseline values. While this ensures sufficient perfusion, intraoperative blood flow monitoring has potential in allowing for patient specific flow rates. Following the procedure,

Biomedical Optics EXPRESS

no significant changes were observed coming off CPB, suggesting no loss of oxygen supply or utilization when restarting the heart. Similarly, no change in S_tO_2 was observed across either transition. Patients also experienced significant drops in total hemoglobin and pH during CPB, while no significant changes in temperature and $PaCO_2$ were observed.

Figure 4 demonstrates the system's ability to capture pulsatile waveforms in the cerebral microcirculation. A patient presented with a bicuspid aortic valve (Fig. 4(A)), which was replaced with an artificial valve (Fig. 4(B)). In the pulse pressure waveform, the first and largest peak represents the systolic phase, corresponding to the aortic valve opening and left ventricular ejection. The second peak visualized represents the vascular elastic recoil following aortic valve closure [32]. After valve replacement, alterations in the height of the curve and shape of the secondary peak were observed. These changes could represent improvements in stroke volume and aortic pressure from cardiac pathologies (e.g., the progressive decrease in aortic pressure due to aortic stenosis) or surgical repairs (e.g. valve integrity) and could provide more insight on the impact of cardiac output on CBF. CPB produces a non-pulsatile blood flow while the heart is arrested. Pulsatile flow has been shown to significantly enhance organ perfusion (i.e. in kidneys) prior to transplant [41], and recent studies investigating non-pulsatile versus pulsatile CPB in major cerebral arteries suggest the potential benefit of cerebral pulsatility [42]; however, there is currently insufficient evidence to necessitate the clinical implementation of pulsatile CPB. Continuous monitoring of CBF and oxCCO could be used to assess the effects of pulsatile versus non-pulsatile CPB on cerebral health.

Throughout surgery, numerous hypoperfusion events caused by large and sustained drops in FR_{CPB} were observed. While on CPB, oxygen supply is solely dependent on the CPB-pump flow rate; reducing FR_{CPB} therefore directly impacts cerebral perfusion and could lead to adverse neurological outcome. Figure 5 displays an example dataset acquired from a patient during a stable period (Fig. 5(A), no notable changes in FR_{CPB}) and during multiple successive drops in FR_{CPB}. Optical metrics during 15 hypoperfusion events (mean drop in FR_{CPB} of $70.6 \pm 28.8\%$ for 93.9 ± 52.5 s) are summarized in Fig. 6 as a function of MAP. As MAP decreased with reduced FR_{CPB}, correlation plots show a consistent decrease in cerebral perfusion, saturation, and metabolism. Statistically significant differences were found for MAP values below 30 mmHg. ΔCBFi showed the earliest response with delayed responses in S_tO_2 and ΔoxCCO. For each event, the maximum change in oxCCO was plotted as a function of the corresponding largest change in CBFi (Fig. 7). Mild-to-moderate reductions in CBFi ($< 70\%$) resulted in small decreases in oxCCO; similar reductions were reported in patients undergoing transaortic valve replacements [43], and in healthy volunteers undergoing hypoxia and hypocapnia challenges [44,45]. Reductions in CBFi $> 70\%$ instigated larger changes in metabolism comparable to reductions observed in infants with brain injury [46]. The adult brain is assumed to have a total CCO concentration of approximately 5.5 µM [18]. The largest observed drop (-1.5 µM) represents an approximate 27% change in oxCCO within the brain. Furthermore, an 18.2 ± 15.0-s delay was observed between metabolic and flow nadirs. Previous studies have shown similar delays in piglets [17,47] and infants [16,33]. Reductions in CBF are likely met by increases in oxygen extraction to maintain stable metabolic levels. Following large and sustained drops in CBF, this compensatory mechanism could become overwhelmed and metabolism impacted. The variability in oxCCO is therefore influenced by the duration of hypoperfusion events observed. While shorter events can elicit similar CBF responses, they may not last long enough to cause the maximum reduction in oxCCO. Further investigations are required to establish clinical thresholds for changes in CBFi and oxCCO in order to understand when values become clinically relevant. Previous work has utilized continuous CBF monitoring to determine a patient-specific lower limit of autoregulation (LLA) [11]. Future work will look to determine the relationship of the LLA with changes in cerebral metabolism.

Biomedical Optics EXPRESS

When translating the optical system to the cardiac operating room, the bright ambient light in the surgical suite was initially a significant source of signal contamination. In this environment, additional shielding in the form of an optical blackout cloth was essential. Further, frequent bed motion and patient repositioning/intervention (i.e. head-cooling with ice, manipulating the transesophageal echocardiography probe) during surgical procedures necessitated strong contact between the optical probes and the surface of the skin. This was achieved by anchoring the optical fibers at a point above the patient, minimizing weight and providing leeway for motion. An additional challenge of the current set-up is the inherent depth sensitivity of the optical technology. The SDDs chosen for B-NIRS and DCS have proven sufficient to interrogate the brain in adult populations [43,48,49]; however, previous work has shown the large contribution from the scalp for NIRS measures [50–52]. While S_tO_2 is susceptible to this effect, oxCCO is less impacted since CCO concentrations are considerably higher in the brain than in extracerebral tissues [18]. To further address depth sensitivity, future work will implement multi-distance measurements to simultaneously acquire scalp perfusion and metabolism and correct for their influence. Previous reports have elaborated on the benefits of measuring extracerebral layers in discerning this contribution [43,49,53,54]. Another future direction will be to modify the system to enable measurements from multiple vascular territories. A limitation with the current system was that the single probe only afforded monitoring in one brain region. In this study, a patient had an intraoperative ischemic stroke in the M1 branch of the right middle cerebral artery, which was not detected by the probes placed on the right side of the forehead. With advancements in lower-cost detector technology, implementing multiple source-detection pairs would enable monitoring across multiple vascular territories [12,55].

5. Conclusion

This study presents the clinical translation and feasibility of an optical neuromonitor capable of continuous measurement of cerebral perfusion and metabolism during cardiac surgery with CPB. Temporal resolution was sufficient to capture physiological responses to transitions on and off the CPB pump and intraoperative hypoperfusion events. Increases in CBFi and significant decreases in MAP and oxCCO were noted during transitions on CPB, with no change during transitions off. Large reductions in CPB-pump flowrate resulted in significant drops in CBFi and oxCCO when MAP decreased below 30 mmHg. The findings regarding metabolic change are supported by previous literature using similar methodologies. The optical system described provides a safe and non-invasive approach for real-time assessment of cerebral hemodynamics and metabolism. More studies are required to determine if direct intraoperative monitoring of CBFi and oxCCO could aid clinicians in patient management and possibly provide insight into the impact of CPB on postoperative cognitive decline and brain injury.

Funding

Natural Sciences and Engineering Research Council of Canada (CHRP 478470); Canadian Institutes of Health Research (CGP-14171); Academic Medical Organization of Southwestern Ontario (INN19-001).

Acknowledgments

The authors would like to acknowledge the patients who participated in this study.

Disclosures

The authors declare no conflicts of interest.

Biomedical Optics EXPRESS

References

1. D. Van Dijk, M. Spoor, R. Hijman, H. M. Nathoe, C. Borst, E. W. L. Jansen, D. E. Grobbee, P. P. T. De Jaegere, and C. J. Kalkman, "Cognitive and cardiac outcomes 5 years after off-pump vs on-pump coronary artery bypass graft surgery," JAMA **297**(7), 701–708 (2007).
2. T. Xu, L. Bo, J. Wang, Z. Zhao, Z. Xu, X. Deng, and W. Zhu, "Risk factors for early postoperative cognitive dysfunction after non-coronary bypass surgery in Chinese population," J. Cardiothorac. Surg. **8**(1), 1–6 (2013).
3. S. Glumac, G. Kardum, and N. Karanovic, "Postoperative cognitive decline after cardiac surgery: A narrative review of current knowledge in 2019," Med. Sci. Monit. **25**, 3262–3270 (2019).
4. G. H. Almassi, T. Sommers, T. E. Moritz, A. L. W. Shroyer, M. J. London, W. G. Henderson, G. K. Sethi, F. L. Grover, and K. E. Hammermeister, "Stroke in cardiac surgical patients: Determinants and outcome," Ann. Thorac. Surg. **68**(2), 391–397 (1999).
5. J. D. Salazar, R. J. Wityk, M. A. Grega, L. M. Borowicz, J. R. Doty, J. A. Petrofski, and W. A. Baumgartner, "Stroke after cardiac surgery: Short- and long-term outcomes," Ann. Thorac. Surg. **72**(4), 1195–1201 (2001).
6. J. P. Gold, M. E. Charlson, P. Williams-Russo, T. P. Szatrowski, J. C. Peterson, P. A. Pirraglia, G. S. Hartman, F. S. F. Yao, J. P. Hollenberg, D. Barbut, J. G. Hayes, S. J. Thomas, M. H. Purcell, S. Mattis, L. Gorkin, M. Post, K. H. Krieger, and O. W. Isom, "Improvement of outcomes after coronary artery bypass: A randomized trial comparing intraoperative high versus low mean arterial pressure," J. Thorac. Cardiovasc. Surg. **110**(5), 1302–1314 (1995).
7. J. M. Murkin, J. K. Farrar, W. A. Tweed, F. N. McKenzie, and G. Guiraudon, "Cerebral autoregulation and flow/metabolism coupling during cardiopulmonary bypass: The influence of PaCO2," Anesth. Analg. **66**(9), 825–832 (1987).
8. U. H. Trivedi, R. L. Patel, M. R. J. Turtle, G. E. Venn, and D. J. Chambers, "Relative changes in cerebral blood flow during cardiac operations using xenon-133 clearance versus transcranial Doppler sonography," Ann. Thorac. Surg. **63**(1), 167–174 (1997).
9. D. Hori, Y. Nomura, M. Ono, B. Joshi, K. Mandal, D. Cameron, M. Kocherginsky, and C. W. Hogue, "Optimal blood pressure during cardiopulmonary bypass defined by cerebral autoregulation monitoring," J. Thorac. Cardiovasc. Surg. **154**(5), 1590–1598 (2017).
10. S. Purkayastha and F. Sorond, "Transcranial doppler ultrasound: Technique and application," Semin. Neurol. **32**(04), 411–420 (2013).
11. J. M. Murkin, M. Kamar, Z. Silman, M. Balberg, and S. J. Adams, "Intraoperative Cerebral Autoregulation Assessment Using Ultrasound-Tagged Near-Infrared-Based Cerebral Blood Flow in Comparison to Transcranial Doppler Cerebral Flow Velocity: A Pilot Study," J. Cardiothorac. Vasc. Anesth. **29**(5), 1187–1193 (2015).
12. M. Diop, E. Wright, V. Toronov, T.-Y. Lee, and K. St Lawrence, "Improved light collection and wavelet de-noising enable quantification of cerebral blood flow and oxygen metabolism by a low-cost, off-the-shelf spectrometer," J. Biomed. Opt. **19**(5), 057007 (2014).
13. A. Casati, G. Fanelli, P. Pietropaoli, R. Proietti, R. Tufano, G. Danelli, G. Fierro, G. De Cosmo, G. Servillo, M. Nuzzi, F. Mentegazzi, A. Fanelli, C. Martani, E. Spreafico, F. Pugliese, P. Aceto, and F. Monaco, "Continuous monitoring of cerebral oxygen saturation in elderly patients undergoing major abdominal surgery minimizes brain exposure to potential hypoxia," Anesth. Analg. **101**(3), 740–747 (2005).
14. J. M. Murkin, S. J. Adams, R. J. Novick, M. Quantz, D. Bainbridge, I. Iglesias, A. Cleland, B. Schaefer, B. Irwin, and S. Fox, "Monitoring brain oxygen saturation during coronary bypass surgery: A randomized, prospective study," Anesth. Analg. **104**(1), 51–58 (2007).
15. D. A. Boas and M. A. Franceschini, "Haemoglobin oxygen saturation as a biomarker: the problem and a solution," Philos. Trans. R. Soc., A **369**(1955), 4407–4424 (2011).
16. A. Rajaram, L. C. M. Yip, D. Milej, M. Suwalski, M. Kewin, M. Lo, J. J. L. Carson, V. Han, S. Bhattacharya, M. Diop, S. de Ribaupierre, and K. St. Lawrence, "Perfusion and Metabolic Neuromonitoring during Ventricular Taps in Infants with Post-Hemorrhagic Ventricular Dilatation," Brain Sci. **10**(7), 452 (2020).
17. A. Rajaram, G. Bale, M. Kewin, L. B. Morrison, I. Tachtsidis, K. St. Lawrence, M. Diop, K. St. Lawrence, and M. Diop, "Simultaneous monitoring of cerebral perfusion and cytochrome c oxidase by combining broadband near-infrared spectroscopy and diffuse correlation spectroscopy," Biomed. Opt. Express **9**(6), 2588–2603 (2018).
18. G. Bale, C. E. Elwell, and I. Tachtsidis, "From Jöbsis to the present day: a review of clinical near-infrared spectroscopy measurements of cerebral cytochrome-c-oxidase," J. Biomed. Opt. **21**(9), 091307 (2016).
19. L. He, W. B. Baker, D. Milej, V. C. Kavuri, R. C. Mesquita, D. R. Busch, K. Abramson, Y. J. Jiang, M. Diop, K. St Lawrence, O. Amendolia, F. Quattrone, R. Balu, W. A. Kofke, and A. G. Yodh, "Noninvasive continuous optical monitoring of absolute cerebral blood flow in critically ill adults," Neurophotonics **5**(04), 1 (2018).
20. T. Pham, K. Tgavalekos, A. Sassaroli, G. Blaney, and S. Fantini, "Quantitative measurements of cerebral blood flow with near-infrared spectroscopy," Biomed. Opt. Express **10**(4), 2117 (2019).
21. T. Durduran, C. Zhou, E. M. Buckley, M. N. Kim, G. Yu, R. Choe, J. W. Gaynor, T. L. Spray, S. M. Durning, S. E. Mason, L. M. Montenegro, S. C. Nicolson, R. A. Zimmerman, M. E. Putt, J. Wang, J. H. Greenberg, J. A. Detre, A. G. Yodh, and D. J. Licht, "Optical measurement of cerebral hemodynamics and oxygen metabolism in neonates with congenital heart defects," J. Biomed. Opt. **15**(3), 037004 (2010).
22. D. Milej, L. He, A. Abdalmalak, W. B. Baker, U. C. Anazodo, M. Diop, S. Dolui, V. C. Kavuri, W. Pavlosky, L. Wang, R. Balu, J. A. Detre, O. Amendolia, F. Quattrone, W. A. Kofke, A. G. Yodh, and K. St Lawrence, "Quantification of

Biomedical Optics EXPRESS

cerebral blood flow in adults by contrast-enhanced near-infrared spectroscopy: Validation against MRI," J. Cereb. Blood Flow Metab. **40**(8), 1672–1684 (2020).
23. D. Wang, A. B. Parthasarathy, W. B. Baker, K. Gannon, V. Kavuri, T. Ko, S. Schenkel, Z. Li, Z. Li, M. T. Mullen, J. A. Detre, and A. G. Yodh, "Fast blood flow monitoring in deep tissues with real-time software correlators," Biomed. Opt. Express **7**(3), 776 (2016).
24. M. Khalid, D. Milej, A. Rajaram, A. Abdalmalak, L. Morrison, M. Diop, and K. St. Lawrence, "Development of a stand-alone DCS system for monitoring absolute cerebral blood flow," Biomed. Opt. Express **10**(9), 4607 (2019).
25. M. Diop, J. Kishimoto, V. Toronov, D. S. C. Lee, and K. St. Lawrence, "Development of a combined broadband near-infrared and diffusion correlation system for monitoring cerebral blood flow and oxidative metabolism in preterm infants," Biomed. Opt. Express **6**(10), 3907 (2015).
26. M. Kewin, A. Rajaram, D. Milej, A. Abdalmalak, L. Morrison, M. Diop, and K. St Lawrence, "Evaluation of hyperspectral NIRS for quantitative measurements of tissue oxygen saturation by comparison to time-resolved NIRS," Biomed. Opt. Express **10**(9), 4789 (2019).
27. A. Duncan, J. H. Meek, M. Clemencet, C. E. Elwellt, and L. Tyszczuk, "Optical pathlength measurements on adult head, calf and forearm and the head of the newborn infant using phase resolved optical spectroscopy," Phys. Med. Biol. **40**(2), 295–304 (1995).
28. M. Essenpreis, C. E. Elwell, M. Cope, P. van der Zee, S. R. Arridge, and D. T. Delpy, "Spectral dependence of temporal point spread functions in human tissues," Appl. Opt. **32**(4), 418 (1993).
29. K. Verdecchia, M. Diop, L. B. Morrison, T.-Y. Lee, and K. St. Lawrence, "Assessment of the best flow model to characterize diffuse correlation spectroscopy data acquired directly on the brain," Biomed. Opt. Express **6**(11), 4288 (2015).
30. P. Lemieux and D. J. Durian, "Investigating non-Gaussian scattering processes by using n th-order intensity correlation functions," J. Opt. Soc. Am. A **16**(7), 1651–1664 (1999).
31. M. Diop, K. Verdecchia, T.-Y. Lee, and K. St Lawrence, "Calibration of diffuse correlation spectroscopy with a time-resolved near-infrared technique to yield absolute cerebral blood flow measurements," Biomed. Opt. Express **2**(7), 2068 (2011).
32. D. M. MacCanon, F. Arevalo, and E. C. Meyer, "Direct Detection and Timing of Aortic Valve Closure," Circ. Res. **14**(5), 387–391 (1964).
33. R. Arora, M. Ridha, D. S. C. Lee, J. Elliott, H. C. Rosenberg, M. Diop, T. Y. Lee, and K. St. Lawrence, "Preservation of the metabolic rate of oxygen in preterm infants during indomethacin therapy for closure of the ductus arteriosus," Pediatr. Res. **73**(6), 713–718 (2013).
34. G. Bale, A. Rajaram, M. Kewin, L. Morrison, A. Bainbridge, M. Diop, K. S. Lawrence, and I. Tachtsidis, "Broadband NIRS Cerebral Cytochrome-C-Oxidase Response to Anoxia Before and After Hypoxic-Ischaemic Injury in Piglets," Oxyg. Transp. to Tissue XL **1072**, 151–156 (2018).
35. M. Taillefer and A. Y. Denault, "Cerebral near-infrared spectroscopy in adult heart surgery: systematic review of its clinical efficacy," Can. J. Anaesth. **52**(1), 79–87 (2005).
36. A. Lassnigg, M. Hiesmayr, P. Keznickl, T. Müllner, M. Ehrlich, and G. Grubhofer, "Cerebral oxygenation during cardiopulmonary bypass measured by near- infrared spectroscopy: Effects of hemodilution, temperature, and flow," J. Cardiothorac. Vasc. Anesth. **13**(5), 544–548 (1999).
37. S. P. Talpahewa, A. T. Lovell, G. D. Angelini, and R. Ascione, "Effect of cardiopulmonary bypass on cortical cerebral oxygenation during coronary artery bypass grafting," Eur. J. Cardio-thoracic Surg. **26**(4), 676–681 (2004).
38. G. W. Fischer, H. M. Lin, M. Krol, M. F. Galati, G. Di Luozzo, R. B. Griepp, and D. L. Reich, "Noninvasive cerebral oxygenation may predict outcome in patients undergoing aortic arch surgery," J. Thorac. Cardiovasc. Surg. **141**(3), 815–821 (2011).
39. G. S. Murphy, E. A. Hessel, and R. C. Groom, "Optimal perfusion during cardiopulmonary bypass: An evidence-based approach," Anesth. Analg. **108**(5), 1394–1417 (2009).
40. A. Wahba, M. Milojevic, C. Boer, F. M. J. J. De Somer, T. Gudbjartsson, J. Van Den Goor, T. J. Jones, V. Lomivorotov, F. Merkle, M. Ranucci, G. Kunst, L. Puis, P. Alston, D. Fitzgerald, A. Nikolic, F. Onorati, B. Steen Rasmussen, and S. Svenmarker, "2019 EACTS/EACTA/EBCP guidelines on cardiopulmonary bypass in adult cardiac surgery," J. Opt. Soc. Am. A **57**(2), ezz267 (2019).
41. C. von Horn and T. Minor, "Isolated kidney perfusion: the influence of pulsatile flow," Scand. J. Clin. Lab. Invest. **78**(1-2), 131–135 (2018).
42. M. P. O. Neil, R. Alie, L. R. Guo, M. Myers, J. M. Murkin, and C. G. Ellis, "Microvascular Responsiveness to Pulsatile and Nonpulsatile Flow During Cardiopulmonary Bypass," Ann. Thorac. Surg. **105**(6), 1745–1753 (2018).
43. T. N. Nguyen, W. Wu, E. Woldemichael, V. Toronov, and S. Lin, "Hyperspectral near-infrared spectroscopy assessment of the brain during hypoperfusion," J. Biomed. Opt. **24**(03), 1 (2019).
44. M. Tisdall, M. Smith, I. Tachtsidis, and C. E. Elwell, "Changes in concentrations of oxidised cytochrome oxidase measured using both broadband and four wavelength near infrared spectroscopy reflect changes in oxygen delivery during hypoxaemia in healthy volunteers," in *Biomedical Optics*, (2006), ME66.
45. L. Holper, J. J. Mann, L. Holper, and J. J. Mann, "Test – retest reliability of brain mitochondrial cytochrome-c-oxidase assessed by functional near-infrared spectroscopy cytochrome-c-oxidase assessed by functional near-infrared spectroscopy," J. Biomed. Opt. **23**(05), 1 (2018).

Biomedical Optics EXPRESS

46. G. Bale, S. Mitra, I. de Roever, M. Sokolska, D. Price, A. Bainbridge, R. Gunny, C. Uria-Avellanal, G. S. Kendall, J. Meek, N. J. Robertson, and I. Tachtsidis, "Oxygen dependency of mitochondrial metabolism indicates outcome of newborn brain injury," J. Cereb. Blood Flow Metab. **39**(10), 2035–2047 (2019).
47. J. A. Cooper, K. M. Tichauer, M. Boulton, J. Elliott, M. Diop, M. Arango, T.-Y. Lee, and K. St Lawrence, "Continuous monitoring of absolute cerebral blood flow by near-infrared spectroscopy during global and focal temporary vessel occlusion," J. Appl. Physiol. **110**(6), 1691–1698 (2011).
48. D. Milej, M. Shahid, A. Abdalmalak, A. Rajaram, M. Diop, and K. St. Lawrence, "Characterizing dynamic cerebral vascular reactivity using a hybrid system combining time-resolved near-infrared and diffuse correlation spectroscopy," Biomed. Opt. Express **11**(8), 4571 (2020).
49. K. Verdecchia, M. Diop, A. Lee, L. B. Morrison, T.-Y. Lee, and K. St. Lawrence, "Assessment of a multi-layered diffuse correlation spectroscopy method for monitoring cerebral blood flow in adults," Biomed. Opt. Express **7**(9), 3659 (2016).
50. J. Selb, D. A. Boas, S.-T. Chan, K. C. Evans, E. M. Buckley, and S. A. Carp, "Sensitivity of near-infrared spectroscopy and diffuse correlation spectroscopy to brain hemodynamics: simulations and experimental findings during hypercapnia," Neurophotonics **1**(1), 015005 (2014).
51. D. Milej, A. Abdalmalak, A. Rajaram, and K. St Lawrence, "Direct Assessment of Extracerebral Signal Contamination on Optical Measurements of Cerebral Blood Flow, Oxygenation, and Metabolism," Neurophotonics, (2020).
52. D. Milej, A. Rajaram, A. Abdalmalak, M. Khalid, M. Shahid, M. Kewin, and K. St. Lawrence, "Assessing extracerebral signal contamination in optical measurements of cerebral blood flow and oxygenation," in Diffuse Optical Spectroscopy and Imaging VII, 90 (2019).
53. T. Sato, I. Nambu, K. Takeda, T. Aihara, O. Yamashita, Y. Isogaya, Y. Inoue, Y. Otaka, Y. Wada, M. Kawato, M. Sato, and R. Osu, "Reduction of global interference of scalp-hemodynamics in functional near-infrared spectroscopy using short distance probes," NeuroImage **141**, 120–132 (2016).
54. A. Gerega, D. Milej, W. Weigl, M. Kacprzak, and A. Liebert, "Multiwavelength time-resolved near-infrared spectroscopy of the adult head: assessment of intracerebral and extracerebral absorption changes," Biomed. Opt. Express **9**(7), 2974 (2018).
55. P. Kaynezhad, S. Mitra, G. Bale, C. Bauer, I. Lingam, C. Meehan, A. Avdic-Belltheus, K. A. Martinello, A. Bainbridge, N. J. Robertson, and I. Tachtsidis, "Quantification of the severity of hypoxic-ischemic brain injury in a neonatal preclinical model using measurements of cytochrome-c-oxidase from a miniature broadband-near-infrared spectroscopy system," Neurophotonics **6**(04), 1 (2019).